

1
2
3 **Low-Frequency Variability in the Gulf of Alaska**
4 **from coarse and eddy-permitting ocean models**
5
6
7
8

9 Antonietta Capotondi¹, Vincent Combes²,
10 Michael A. Alexander³, Emanuele Di Lorenzo², and Arthur J. Miller⁴
11
12
13
14
15
16

17 ¹ NOAA/ESRL/PSD, and University of Colorado/CIRES, Boulder, CO

18 ² School of Earth and Atmospheric Sciences, Georgia Institute of Technology, Atlanta, GA

19 ³ NOAA/ESRL/PSD

20 ⁴ Scripps Institute of Oceanography, La Jolla, CA
21
22
23
24
25

26 Corresponding Author Address:

27
28 Antonietta Capotondi

29 NOAA/ESRL/PSD

30 325 Broadway

31 Boulder, CO 80305
32

33 Antonietta.Capotondi@noaa.gov
34
35
36
37
38
39
40
41
42

Abstract

An eddy-permitting ocean model of the northeast Pacific is used to examine the ocean adjustment to changing wind forcing in the Gulf of Alaska (GOA) at interannual-to-decadal timescales. It is found that the adjustment of the ocean model in the presence of mesoscale eddies is similar to that obtained with coarse-resolution models. Local Ekman pumping plays a key role in forcing pycnocline depth variability and, to a lesser degree, SSH variability in the center of the Alaska gyre and in some areas of the eastern and northern GOA. Westward Rossby wave propagation is evident in the SSH field along some latitudes, but is less noticeable in the pycnocline depth field. Differences between SSH and pycnocline depth are also found when considering their relationship with the local forcing and leading modes of climate variability in the northeast Pacific. In the central GOA pycnocline depth variations are more clearly related to changes in the local Ekman pumping than SSH. While SSH is marginally correlated with both Pacific Decadal Oscillation (PDO) and North Pacific Gyre Oscillation (NPGO) indices, the pycnocline depth evolution is primarily related to NPGO variability. The intensity of the mesoscale eddy field increases with increasing circulation strength. The eddy field is generally more energetic after the 1976-77 climate regime shift, when the gyre circulation intensified. In the western basin, where eddies primarily originate from intrinsic instabilities of the flow, variations in eddy kinetic energy (EKE) are statistically significant correlated with the PDO index, indicating that eddy statistics may be inferred, to some degree, from the characteristics of the large-scale flow.

65

66 **1. Introduction**

67

68 The pycnocline, the layer characterized by large vertical density gradients, plays a
69 central role in the dynamical processes of the Gulf of Alaska (GOA). In this region the
70 pycnocline has a doming structure, being shallower in the central part of the gulf, and
71 deeper along the coast. The horizontal gradients of pycnocline depth determine the
72 direction and intensity of the geostrophic currents, and the doming shape of the
73 pycnocline is consistent with the anticyclonic gyre circulation. The GOA has an upper
74 ocean structure characterized by a thick layer of low salinity near the surface. Since at
75 high-latitudes salinity has a dominant control upon density, the halocline, the depth with
76 the largest salinity gradients determines the pycnocline. In winter, the mixed layer
77 reaches to the top of the pycnocline, so that pycnocline variability is closely related to
78 changes in the winter mixed layer depth (MLD, [Freeland *et al.*, 1997]), a quantity that
79 has a large influence upon biological processes in the GOA. Thus, pycnocline variability
80 is very important for both the physics and the biology of the GOA.

81 Previous studies [Lagerloef, 1995; Cummins and Lagerloef, 2004; Capotondi *et al.*,
82 2005, CADM05 hereafter] have stressed the role of the Ekman pumping for driving
83 pycnocline depth changes. Local Ekman pumping forcing can explain a large fraction of
84 pycnocline variability observed at Ocean Weather Station Papa (Papa hereafter,
85 [Cummins and Lagerloef, 2002]) in the center of the gyre. Using a non eddy-resolving
86 ocean model forced with observed surface fields over the period 1958-1997 CADM05
87 showed that local Ekman pumping could account for most of the pycnocline variability in
88 the whole offshore region of the GOA, while in a broad band following the coast the

counterclockwise propagation of pycnocline depth anomalies seemed to be the controlling process.

Analyses of satellite altimeter data over the period 1993-2000 [Qiu, 2002] suggest that variations in sea surface height (SSH) in the offshore region of the Gulf of Alaska cannot simply be accounted for by local Ekman pumping, but the inclusion of westward propagation is essential to capture a significant fraction of the SSH variations. Is the discrepancy between the findings of Qiu [2002] and CADM05 due to the coarse resolution of the model used by CADM05, and the lack of mesoscale variability and coastal processes in that model, or could pycnocline depth and SSH contain slightly different dynamical information?

Recent studies [Di Lorenzo *et al.*, 2008; Chhak *et al.*, 2008] have shown that variations in many aspects of the upper ocean in the northeast Pacific, including sea surface temperature (SST), sea surface height (SSH), and sea surface salinity (SSS) are controlled by large-scale atmospheric forcing and are significantly correlated with two leading modes of climate variability. These modes have recently been defined by Di Lorenzo *et al.* [2008] as the leading Empirical Orthogonal Functions (EOFs) of the SSH field over the region 180°W – 110°W, 25°N – 62°N, based on a 50-year model hindcast. The first mode, which is characterized by a large anomaly centered around 160°W, 40°N, and anomalies of opposite polarity along the coast, has been termed the Pacific Decadal Oscillation (PDO) by Di Lorenzo *et al.* [2008] due to its similarity with the leading EOF of monthly SST anomalies over the North Pacific computed by Mantua *et al.* [1997].

The second mode of variability has a dipole structure, with a nodal line approximately along 40°N, and anomalies of opposite polarity corresponding to an intensification of the

eastern and central branches of the North Pacific subpolar and subtropical gyres, and hence termed the North Pacific Gyre Oscillation (NPGO) mode. The principal component (PC) of the NPGO mode, or NPGO index, is highly correlated with the second PC of SST anomalies [Bond *et al.*, 2003], known as the “Victoria Mode”. While the PDO mode can explain a large fraction of the SST and SSH variability in the northeast Pacific, the NPGO mode appears to be highly correlated with SSS variations, as well as nutrient upwelling and surface chlorophyll-a [Di Lorenzo *et al.*, 2008, Chhak *et al.*, 2008].

Climate change over the next century can be expected to alter the dominant modes of climate variability, and their influence upon the northeast Pacific circulation. The primary means available for predicting the nature of those changes are state-of-the-art climate models, whose present resolution does not capture several regional processes, including coastal topographic waves and mesoscale variability. Mesoscale eddies play a fundamental role in transport and mixing processes [Crawford *et al.*, 2005; 2007; Ladd *et al.* 2005], with important implications for both the large-scale circulation and ecosystem dynamics. While the details of the mesoscale eddy field is not reproduced by the current generation of climate models, the statistics of the mesoscale eddy field may be related to some aspects of the large-scale circulation, so that knowledge of the circulation response to climate change may provide useful insights into eddy statistics changes. Thus, it is important to examine how well models with the resolution typically used for climate simulations can represent the main aspects of the large-scale ocean circulation in the GOA, and the processes governing its variability. It is also important to clarify the relationship between large-scale circulation and the statistics of sub-grid scale processes.

As a first step to elucidate the ability of climate models to represent the physical processes involved in the GOA circulation variability we revisit the issues examined by CADM05 in the context of an eddy-permitting, regional model of the northeast Pacific region. Our purpose in this study is twofold: 1) clarify the influence of resolution in modeling the leading dynamical processes controlling changes in pycnocline depth in the Gulf of Alaska, and 2) compare the dynamical information contained in pycnocline depth with that obtained from SSH data, and examine the relationship between the two fields. Specific questions we ask are: 1) To what extent can the local Ekman pumping explain pycnocline and SSH variability in the presence of intrinsic ocean variability?, and 2) Is eddy statistics in the GOA related to the large-scale circulation and to the major modes of North Pacific climate variability?

The paper is organized as follows: in section 2 we describe the model simulations and the data used to validate the models. In section 3 we examine the changes in pycnocline depth and SSH that characterize the 1976-77 climate shift in both low-and high-resolution models. In section 4 we compare the ability of the Ekman and Rossby wave models to reproduce the changes in pycnocline depth and SSH in the high-resolution model and in satellite observations. and in section 5 a summary is offered, and conclusions are drawn.

2. Models and data

The main model used for this study is the Regional Ocean Modeling System (ROMS, [Haidvogel *et al.*, 2000; Shchepetkin and McWilliams, 2005; Curchitser *et al.*, 2005]). The model domain extends from 25°N to 60°N, and from 180°W to 110°W with a horizontal resolution from 19km in the southern part of the domain to 13.4km in the

northern part of the domain. While the resolution of the model is an improvement with respect to coarse resolution models, it is only comparable to the internal deformation radius in the GOA, which ranges from 16–18 km in the open ocean GOA [Chelton *et al.*, 1998] to 10 km over some shelf regions. Thus, the model is eddy-permitting, but not fully eddy-resolving. Higher resolution models that test the sensitivity of solutions to changes in frictional parameterizations, topographic smoothing, inflow conditions, radiation boundary conditions and surface forcing need to be examined to determine the robustness of our results. There are 30 vertical levels, with higher resolution near the surface.

The model is initialized using temperature, salinity, horizontal velocities, and SSH derived from *Levitus* [1994]. At the model open boundaries a modified radiation boundary condition [Marchesiello *et al.*, 2001] is prescribed, to allow perturbations excited within the model domain to propagate out of the domain, together with nudging of the model temperature, salinity and geostrophic velocities (relative to 1000m) fields toward the monthly climatological values derived from *Levitus* [1994]. Thus, no perturbation can enter the domain through the open boundaries. In particular, this prevents coastal Kelvin waves of equatorial origin, excited during ENSO events, from propagating northward into the domain, a process that can be a source of interannual variability along the coastal waters of the GOA [Enfield and Allen, 1980; Chelton and Davis, 1982; Emery and Hamilton, 1985; Meyers and Basu, 1999; Qiu, 2002]. This is an aspect in which the ROMS simulation differs from the simulation analyzed by CADM05. As described later in this section, the model used by CADM05 is global, includes ENSO variability, and disturbances of equatorial origin can propagate northward along the coast.

Comparison of model-derived time series of SSH at coastal locations where observations are available (Neah Bay, Sitka, Yakutat, Seward, Kodiak, and Sand Point) by *Combes and Di Lorenzo* [2007, CDL07 hereafter] shows that the model can explain a significant fraction of the interannual (mean seasonal cycle removed) variance of the observed time series, indicating that wave propagation from the equator does not play the dominant role in interannual variations along the GOA coast. These interannual variations in SSH and pycnocline depth result from both upstream propagation and local forcing [*Qiu*, 2002; CADM05].

The model was first spun-up for 80 years, using monthly climatological forcing and restoring boundary conditions for surface temperature and salinity. The experiment we examine in the present study starts at the end of the spin-up, and is driven by surface wind stresses from the National Center for Environmental Prediction/National Center for Atmospheric Research (NCEP/NCAR) over the period 1950-2004 [*Kalnay et al.*, 1996], surface heat fluxes corrected using the National Oceanographic and Atmospheric Administration (NOAA) extended SST [*Smith and Reynolds*, 2004], and monthly climatological freshwater fluxes diagnosed from the spin-up experiment. Two additional simulations, each starting at the end of the previous 55-year run, have been carried out, providing three ensemble members that can offer a way to discriminate between externally forced and internal model variability (CDL07). Unless explicitly stated, the analysis performed in this study will focus on the third ensemble member, which can be expected to have a more adjusted deep ocean. In spite of differences between the members due to the model internal variability, the main results do not change significantly when different members are considered.

The ROMS model simulation will be compared with the results of CADM05 based on the output from the NCAR ocean model (NCOM), a global ocean model derived from the Geophysical Fluid Dynamics Laboratory (GFDL) Modular Ocean Model (MOM). NCOM has been described in detail in *Large et al.* [2001]. The specific simulation analyzed by CADM05 has been described by *Doney et al.* [2003]. The model resolution is 2.4° in longitude and 1.2° in latitude in the GOA. The NCOM simulation analyzed by CADM05 was forced with wind stresses from the NCEP/NCAR Reanalysis over the period 1958-1997. Sensible and latent heat fluxes were computed from the NCEP winds and relative humidity and the model's SSTs using air-sea transfer equations [*Large and Pond*, 1982; *Large et al.*, 1997]. Precipitation information was obtained by combining microwave sounding unit (MSU) monthly observations [*Spencer*, 1993] and *Xie and Arkin* [1996] observations from 1979 to 1993, while monthly climatologies of the two datasets are used prior to 1979. From 1993 to 1997 MSU values are used in the tropical Pacific and Indian Oceans, as well as along the Alaskan coast, where the Xie-Arkin values are believed to be too large, while the Xie-Arkin data are used everywhere else.

In spite of differences in the way surface heat and freshwater fluxes are prescribed, the ROMS and NCOM simulations have comparable wind forcing, which appears to be a fundamental component in driving upper-ocean variability in the GOA [*Lagerloef*, 1995; *Cummins and Lagerloef*, 2002; CADM05; CDL07]. However, ROMS and NCOM have very different horizontal resolutions, and can be used to examine the role of internal model variability on the leading dynamical processes involved in the ocean adjustment to changing wind forcing. Unlike ROMS, which has a free-surface, NCOM applies the rigid lid approximation, so that SSH information is not available from the model output.

Data used to validate the models include time series of pycnocline depth at Ocean Weather Station Papa (50°N, 145°W, Papa hereafter), and at station GAK1 (149°W, 59°N). These time series are sufficiently long to assess the simulated variability and the changes across the 1976-77 climate shift. Papa provides a long record of bottle cast and CTD data over the period 1957-94. The time series has been recently augmented by more recent observations from 1995 to 1999. Generally, the density of observations is higher in the earlier period, 1957-81, when the station was occupied on a regular basis by the weather ship.

GAK1 is located at the mouth of Resurrection Bay near Seward, Alaska. Profiles of temperature and salinity to a depth of 250 meters have been measured starting in December 1970. The number of winter (December-April) observations varies from year to year ranging from less than 5 measurements in 1972, 1980, 1981, and 1985 to a maximum of 15 values in 1999. The depth of the pycnocline was estimated by CADM05 using individual profiles, and then averaged over the winter season. Both time series are compared with similar time series from the models, which are based on monthly means of values produced by the model at each time step, typically a few hours.

Altimetric observations of SSH derived from the AVISO (Archiving, Validation and Interpretation of Satellite Oceanographic data, Centre National d'Etudes Spatiales) maps are used to validate aspects of ROMS SSH. The AVISO maps combine data from the Topex/Poseidon, JASON-1, ERS-1/2, and Envisat satellites to produce sea level anomalies at weekly resolution from October 1992 to January 2005 on a $1/3^\circ \times 1/3^\circ$ Mercator grid [Ducet et al., 2000; Le Traon and Dibarboure, 1999]. Here we use

monthly averages of the SSH from the AVISO product for consistency with the monthly averaged model output.

3. The 1976-77 climate shift

a. Circulation changes

The 1976-77 climate regime shift had profound impacts on both the physics and the biology of the GOA [Nitta and Yamada, 1989; Trenberth and Hurrell, 1994; Yasuda and Hanawa, 1997], thus providing an important case study for comparing the differences in upper-ocean structure and circulation simulated by models with different resolutions, as well as for examining variations in eddy statistics associated with different ocean “regimes”. The changes associated with the 1976-77 regime shift in the models have been computed as the difference between a period after the shift (P2, 1977-1997), and a period before the shift (P1, 1958-1975). The choice of the two periods has been motivated by two factors: first, we want to compare the changes in ROMS with those in NCOM, so that we need to consider periods available from both simulations. Second, since another climate shift occurred in 1998 [Bond *et al.*, 2003], it seems preferable to exclude the period after 1998 from this analysis.

Within the ROMS simulation we will examine both changes in SSH and pycnocline depth. The mean patterns of SSH and pycnocline depth (h) over the total duration of the integration are shown in Figure 1. The depth of the $27.0 \sigma_\theta$ isopycnal is chosen here as a proxy for pycnocline depth. Both fields in Figure 1 show large horizontal gradients along the western margin of the GOA, where the Alaskan Stream flows. SSH deepens in the interior, where the pycnocline becomes shallower, so that the two fields are

approximately the mirror image of each other, with proper scaling. The spatial structure of the mean pycnocline depth and SSH is in good qualitative agreement with the dynamic height field computed by *Crawford et al.* [2007], based on their compilation of all archived hydrographic measurements over the period 1929-2005.

The Ekman pumping is one of the primary drivers of the circulation in the GOA. The changes in Ekman pumping associated with the 1976-77 climate shift (Figure 2) show a broad band along the eastern and northern margins of the GOA, all the way to Kodiak Island (marked with a “K” in Figure 2), where the Ekman pumping becomes more downwelling favorable (negative values) after the shift, while in the central and western GOA the Ekman pumping change is positive, creating more upwelling favorable conditions. Downwelling along the eastern GOA increases the horizontal gradients of SSH and pycnocline depth along the eastern margin, resulting in an intensification of the Alaska Current (CDL07).

The change in pycnocline depth after the 1976-77 climate shift in the NCOM simulation, computed as the difference between P2 and P1, shows deepening of the pycnocline in a broad band along the coast, and shoaling of the pycnocline in the center of the Alaska Gyre (Figure 3a). A qualitatively similar pattern is also found in the ROMS simulation (Figure 3b), with deeper pycnocline along the coast, and shallower pycnocline away from the coast, a pattern that is consistent with an intensification of the Alaska gyre after the shift, as described by CADM05. However, several differences can be observed. The changes in pycnocline depth between P1 and P2 are much smaller in ROMS than in NCOM. While the pycnocline depth changes by 15-20m in NCOM, the depth changes in ROMS are less than 10m. The spatial pattern of the changes is also quite different, as the

negative values in ROMS are primarily limited to a zonal band between 45°N and 52°N. The pycnocline depth changes in most of the domain are consistent with the sign of the Ekman pumping changes (Figure 2). In particular, the deepening of the pycnocline along the eastern and northern margins of the GOA is in agreement with the more downwelling favorable conditions in those areas after the shift. Similarly, the shoaling of the pycnocline in the central GOA is consistent with the more upwelling favorable Ekman pumping after 1977. However, southwest of Kodiak Island, along the Alaska Peninsula and the Aleutian Islands the pycnocline deepens in spite of the positive Ekman pumping change, as also found by CADM05.

Are the changes in SSH associated with the 1976-77 climate regime shift similar to the changes in pycnocline depth? The difference in the SSH field ($P2 - P1$) is shown in Figure 3c. The values of SSH are converted to pycnocline depth units by multiplying them by the ratio of the acceleration of gravity and the reduced gravity, as described in section 4 (equation 5). The SSH difference also shows positive values along the coast and negative values in the interior, in qualitative agreement with the pattern of pycnocline depth changes. However, the positive SSH values along the eastern Gulf of Alaska extend further into the interior than the positive anomalies of pycnocline depth, and the negative SSH difference in the interior appears displaced westward with respect to the pycnocline depth difference in ROMS, as well as NCOM. As a result, at the location of station Papa (145°W, 50°N, “P” in Figure 3a) a shoaling of the pycnocline can be expected from both NCOM and ROMS, but no significant change in SSH seems to occur at that location based on the ROMS results. The maximum differences in Figure 3c are

larger than those in Figure 3b, and more in line with the pycnocline depth changes in NCOM, although significant SSH changes are only found north of 45°N.

CADM05 compared the evolution of pycnocline depth from NCOM with that observed at Papa and GAK1 (“G” in Figure 3a). As seen in Figure 3a, the two stations are in the shoaling and deepening pycnocline regions, respectively. Here we perform a similar comparison for the ROMS fields (Figure 4). The time series of pycnocline depth at Papa from ROMS shows a similar evolution to that from NCOM (Figure 4a), especially before 1980. The large shoaling event (negative depth anomaly) observed at Papa in 1983-84 is underestimated by the models, especially ROMS, while the negative anomaly in 1989 is largely overestimated by ROMS. The correlation coefficients of the ROMS and NCOM pycnocline depth time series with the observed time series at Papa are 0.42 and 0.61, respectively. Both correlation coefficients are significant at the 95% level.

Similar agreement is found at GAK1 (Figure 4b), where the correlation coefficients of the ROMS and NCOM time series with the observed are 0.61 and 0.65, respectively. Notice that neither NCOM nor ROMS reproduce the high variance observed at GAK1, while the variance of the modeled time series is more comparable with that derived from observations at Papa. One possible explanation is that Papa is in the open ocean, while GAK1 is on the shelf, where models, especially NCOM, may be limited by resolution in their ability to simulate pycnocline variability. Another important factor is sampling. While the values of pycnocline depth anomalies at GAK1 are the average of very few winter observations, the model values are derived from monthly averages which likely give rise to smoother time series.

The time series of SSH are compared with the time series of pycnocline depth observed at Papa and GAK1 in Figures 4c, 4d. The time series of SSH from ROMS are multiplied by the ratio of gravity and reduced gravity (equation 5 in section 4) to convert them to pycnocline depth units. At Papa (Figure 4c), the correlation coefficient between SSH from ROMS and the observed pycnocline depth is only 0.05, reflecting large discrepancies between the two time series. Before 1980, all the negative events are more pronounced in the SSH time series from ROMS than in the observations. A particularly large discrepancy is the negative event around 1970, which is found in the SSH evolution, but not in the pycnocline depth evolution from ROMS (Figure 4a). A better correspondence between SSH from ROMS and observed pycnocline depth is found at GAK1, where the correlation coefficient between SSH from ROMS and observed pycnocline depth is 0.59, a value statistically significant at the 95% level.

b. The mesoscale eddy field

Given the importance of mesoscale eddies for transport processes and ecosystem dynamics in the GOA we examine whether the changes in circulation after the 1976-77 climate regime shift were associated with significant changes in eddy statistics. A preliminary attempt to address this issue was carried out by *Miller et al.* [2005], using an earlier version of the ROMS model. The processes responsible for eddy generation and evolution are somewhat different in the eastern and western regions of the GOA (CDL07, and references therein). The mesoscale eddy field in the northern and eastern Gulf of Alaska primarily consists of three groups of anticyclonic eddies: the Haida eddies which

form close to Queen Charlotte Island (“Q” in Figure 2, [Crawford, 2002]), the Sitka eddies, generated offshore of the town of Sitka (“S” in Figure 2, [Tabata, 1982]), and the Yakutat eddies in the northern gulf (“Y” in Figure 2). Since these eddies are generated by instabilities of the coastal current as it interacts with topographic features, an increase in the strength of the Alaska Current tends to lead to increased eddy generation [Crawford *et al.*, 2002; CDL07]. In the eastern basin the pycnocline depth and its horizontal gradients, which, by geostrophy, determine the intensity of the Alaska Current, are controlled primarily by the local winds (CDL07). Thus, eddy generation is also related to the local winds, and considered somewhat deterministic [Okkonen *et al.*, 2003].

In contrast, some of the eddies observed in the western basin along the Alaskan Stream propagate from the eastern and northern eddy formation areas, while others form along the Stream [Crawford *et al.*, 2000, Ladd *et al.*, 2007; Ladd, 2007]. Eddy generation along the Stream appears to be associated with internal instabilities of the flow, so that these eddies cannot directly be related to the local wind forcing [Okkonen, 2001]. Eddies propagating into the western basin along the margin of the GOA will have a lagged correlation with the winds in the formation areas.

CDL07 has examined the relationship between eddy variance and wind forcing by comparing the same ROMS simulation analyzed here with a simulation forced by monthly climatological fields. On interannual timescales, the forced simulation yields larger eddy variance in the eastern basin, while the variance in the western basin does not show significant differences between the two runs. Moreover, when the three model ensemble members are considered, it is found that the evolution of SSH anomalies is very similar among ensemble members in the Haida and Sitka eddy formation sites, while a

large spread is found in the evolution of SSH along the Alaskan Stream, suggesting a dominance of internal vs. forced variations in the western basin in the model (CDL07).

The issue that we address here is whether a relationship can be found between eddy variance and intensity of the gyre circulation. Differences of standard deviations of SSH and pycnocline depth (Figure 5) between the period after the shift and the period before the shift show larger values after 1977 in both the eastern and western margins. The larger standard deviations along the coast are much more evident in the SSH than in the pycnocline depth field, for our choice of P1 and P2. In the eastern basin, localized maxima are found offshore of Queen Charlotte Island (53°N, 130°W), where the Haida eddies are formed, while offshore of Sitka (57°N, 135°W) small areas of both increased and decreased variance are found. Enhanced variance is also detected around the apex of the gulf, where the Yakutat eddies are generated. Away from the coastal region, a broad band of increased variance is found between 155°W and 135°W, south of ~48°N. This area is not associated with large mean variance (not shown). The increased variability in both SST and pycnocline depth after the climate shift in this region may be associated with increased variance in the wind forcing.

To further quantify the relationship between eddy statistics and gyre circulation, we examine the evolution of eddy kinetic energy (EKE) in the ROMS simulation. To place the pattern of EKE in the context of the gyre circulation, we start by computing the surface total kinetic energy (TKE):

$$TKE = 0.5 * (u^2 + v^2), \quad (1)$$

where u and v are the total surface velocities from the ROMS simulations, available at a monthly time resolution. The time mean TKE, averaged over the total duration of the

integration (Figure 6a) maximizes in the area of the Alaskan Stream in the western GOA, but values larger than $100 \text{ cm}^2\text{s}^{-2}$ are also found on the eastern and northern part of the basin, offshore of Queen Charlotte Island, and from Sitka to the apex of the gulf following the coast. The EKE is computed using equation (1) after removing the long-term mean from the velocities. The pattern of mean EKE (Figure 6b) also shows localized maxima in the area of Queen Charlotte Island and Sitka, where the Haida and Sitka eddies are formed, with maximum values of $\sim 80 \text{ cm}^2\text{s}^{-2}$, and a broad area of values larger than $60 \text{ cm}^2\text{s}^{-2}$ to the southwest of the core of maximum TKE. To assess the degree of realism of the EKE pattern from ROMS, we compute EKE from the AVISO altimeter data, based on monthly averaged SSH anomalies (long-term mean removed):

$$EKE_{AVISO} = 0.5 * (u_g'^2 + v_g'^2), \quad (2)$$

where u_g' and v_g' are the geostrophic velocities estimated from the AVISO SSH:

$$u_g' = -\frac{g}{f} \frac{\Delta\eta'}{\Delta y}, v_g' = \frac{g}{f} \frac{\Delta\eta'}{\Delta x}, \quad (3)$$

with g being the acceleration of gravity, and f denoting the Coriolis parameter. The pattern of EKE from AVISO, relative to the period 1993-2004 (Figure 6c) is very similar to that computed by *Ladd* [2007] from weekly sea level anomalies (SLA), but the maximum values in Figure 6c are smaller than those in *Ladd* [2007], due to the monthly averaging. Comparison of Figures 6b and 6c shows several discrepancies between the modeled and observation-derived EKE patterns. The maximum EKE extending from Sitka to the west of the apex of the gulf, where the Yakutat eddies are formed is missing in the model, suggesting that the generation of Yakutat eddies, as well as the westward propagation of the eastern eddies along the coast [*Crawford et al.*, 2000; *Ladd*, 2007] are not correctly captured by the model. The large values of EKE in the western margin of

the GOA are confined within a much narrower band in the map from the altimeter than in the model. The values of EKE in the model are also generally lower than those estimated from the altimetric observations, a result likely due to the eddy-permitting (and not fully resolving) nature of this ROMS simulation.

The changes in EKE associated with the 1976-77 climate shift, as estimated from ROMS as the difference between P2 and P1 (figure 6d) have a noisy structure, showing an overall increase in EKE along the coast after the shift, with some localized areas where the EKE decreased after 1977. Since the western GOA eddies seem to originate primarily from internal instability of the Alaskan Stream in the model, we compute an EKE index by averaging the EKE over the area where the TKE is larger than $100 \text{ cm}^2\text{s}^{-2}$ in the western basin (between 165°W and 148°W , and north of 52°N). After removing the monthly means and smoothing the EKE time series with a 3-point binomial filter, we compare the evolution of the EKE index with both the PDO and NPGO indices (Figure 7).

The correlation coefficient between EKE in the western basin and the PDO is 0.54, which is statistically significant at the 99% level. The correlation with the NPGO index, on the other hand, is only 0.22, whose statistical significance is below the 90% level. CDL07 has shown that the PDO index was statistically significant correlated with the Principal Component (PC) of the leading Empirical Orthogonal Function (EOF) of SSH from the same model simulation, a mode of variability corresponding to variations in the gyre strength. Thus, although unrelated with the local wind forcing, eddy activity in the western GOA increases with increasing gyre circulation strength. The statistically significant correlation between EKE in the western basin and PDO index is consistent

with the large coherent loading of the PDO mode along the coast. While the correspondence between eddy production and circulation strength is relatively well established in the eastern and northern basin [Crawford *et al.*, 2002; CDL07; Ladd, 2007], much less is known for the western eddies. Here we show that western eddies are also related to some large-scale mode of climate variability and the associated circulation variations. This suggests that if climate models can successfully simulate the major modes of climate variability and the associated changes in the large-scale ocean circulation, eddy statistics could be partially inferred from those circulation changes.

4. Ekman vs. Rossby wave dynamics

To elucidate the dynamical processes involved in the ocean adjustment to varying wind forcing we use the Ekman pumping and Rossby wave models considered by CADM05 and Qiu [2002]. These models have proved very useful in accounting for a large fraction of pycnocline depth and SSH variability at interannual and longer timescales in the northeast Pacific [Lagerloef, 1995; Cummins and Lagerloef, 2002; 2004], but the relative role of local Ekman pumping forcing vs. westward Rossby wave propagation is not entirely clear.

The Ekman pumping model:

$$\frac{dh}{dt} = -W_E - \lambda h, \quad (4)$$

relates the time rate of change of the pycnocline depth h to the Ekman pumping W_E in the presence of dissipation, as described by a linear damping term with coefficient λ . A similar equation can be derived for SSH using a two-layer approximation for the ocean

475 [Qiu, 2002]. Assuming that the bottom layer is much deeper than the top layer, the SSH
 476 (ζ) is related to the pycnocline depth:

$$477 \quad \zeta = (g'/g)h, \quad (5)$$

478 where g' is the reduced gravity, $g' = (\rho_2 - \rho_1)g/\rho_o$, with ρ_1 and ρ_2 the densities of the top
 479 and bottom layers, respectively, and ρ_o is the mean density of seawater. The Ekman
 480 pumping is the vertical velocity at the base of the Ekman layer due to the divergence of
 481 the Ekman currents, and is defined as the vertical component of the curl of the wind
 482 stress τ divided by the Coriolis parameter f and the mean density of seawater ρ_o :

$$483 \quad W_E = \left[\nabla \times \left(\frac{\tau}{\rho_o f} \right) \right]. \quad (6)$$

484 Monthly values of W_E from the NCEP-NCAR reanalyses, the same forcing that drives
 485 the ROMS simulation, are used to force (4). Equation (4) is solved using a second-order
 486 accurate trapezoidal scheme as:

$$487 \quad h^{n+1} = \alpha_1 h^n + \alpha_2 W_E^{n+1/2}, \quad (7)$$

488 where $\alpha_1 = (2 - \lambda\Delta t)/(2 + \lambda\Delta t)$, $\alpha_2 = (2\Delta t)/(2 + \lambda\Delta t)$, and $W_E^{n+1/2}$ is the average Ekman
 489 pumping at times n and $n+1$. The initial condition for (4) is the pycnocline depth (or
 490 SSH) at the initial time (January 1950). The value of λ at each grid point has been
 491 defined as in CADM05 as the value that maximizes the correlation between pycnocline
 492 depth (or SSH) from the simple model (4) and that from ROMS. The maximum
 493 correlations (as function of λ) are shown in Figure 8 for both pycnocline depth (Figure
 494 8a) and SSH (Figure 8c).

The correlation pattern is very similar to that computed by CADM05 (their Figure 6b) with the largest values in the center of the gulf and very low correlations in a band along the western margin. As seen in section 3, the Ekman pumping anomalies associated with the 1976-77 climate shift are upwelling favorable southwest of Kodiak Island and the Alaska Peninsula (Figure 2), while the pycnocline is deeper after the shift in that area (Figure 1). The spatial structure of Ekman pumping variations associated with the regime shift in the mid-seventies is similar to the leading EOF of interannual Ekman pumping anomalies [Cummins and Lagerloef, 2002]. Pycnocline depth variations along the western side of the Gulf of Alaska are not forced by the local Ekman pumping, thus explaining the low correlations in Figure 8 in that area.

The correlation patterns in Figures 8a, c although broadly similar to that computed by CADM05, shows more small scale features than the corresponding pattern of CADM05, due to the eddy-permitting nature of ROMS. ROMS correlations are also generally lower than those computed using NCOM, especially the SSH correlations (Figure 8c). Notice the coastal area of relatively large correlations from north of Queen Charlotte Island to the apex of the gulf in both Figures 8a, c. That is an area where the anomalous Ekman pumping associated with the 1976-77 climate shift is downwelling favorable, and has a center of action centered around 140°W, 56°N (Figure 2).

The right panels in Figure 8 show the values of λ^{-1} that maximize the correlation between the evolution of the h (Figure 8b) and SSH (Figure 8d) fields in ROMS and the corresponding fields from the Ekman pumping model. Values are shown only over the areas where the correlations are larger than 0.5. Despite the noisy spatial pattern of λ^{-1} , in the central GOA, where correlations are larger, λ^{-1} is ~10-20 months, in agreement with

the findings of CADM05, as well as the value of 17 months found by Cummins and Lagerloef (2002) at Papa, using statistical methods.

Qiu [2002] has shown that the temporal evolution of SSH anomalies from TOPEX/Poseidon altimetry (October 1992 – July 2000) was well described by a dynamical framework that included westward propagation of the anomalies at the speed of first-mode baroclinic Rossby waves. The model for the evolution of pycnocline depth in the presence of Rossby wave propagation h_R can be written as:

$$\frac{\partial h_R}{\partial t} + c_R \frac{\partial h_R}{\partial x} = -W_E - \lambda_1 h_R, \quad (8)$$

where $c_R = -\beta R^2$ is the phase speed of long baroclinic Rossby waves, a function of the Rossby radius of deformation R , and the latitudinal gradient of the Coriolis parameter β . λ_1 is a Rayleigh friction coefficient, which, following CADM05 has been chosen to be $(4\text{yr})^{-1}$. The Rossby wave phase speed is latitude dependent, decreasing with increasing latitude, and is also influenced by the background mean flow [*Killworth et al.*, 1997]. Following *Killworth et al.* [1997], we have chosen $c_R \approx 0.8 \text{ cm s}^{-1}$ along 50°N . Equation (8) can be solved by integrating along Rossby wave characteristics in the x - t plane:

$$h_R(x, t) = h_R(x_E, t - t_E) e^{-\lambda_1 t_E} + \int_{x_E}^x \frac{W_E(\xi, t - t_\xi)}{c_R(\xi)} e^{-\lambda_1 t_\xi} d\xi. \quad (9)$$

The solution at point x and time t is the superposition of two terms: the first term on the rhs of (9) is the contribution of disturbances originating at the eastern boundary x_E and reaching point x at time t with a transit time $t_E = \int_{x_E}^x d\xi / c_R(\xi)$; the second term on the rhs of (9) is the contribution of the anomalies excited by the Ekman pumping east of

539 the target point x , with $t_\xi = \int_\xi^x ds/c_R(s)$ being the transit time from point ξ to point x .

540 Both boundary and wind-forced terms decay while propagating westward with an e-
541 folding time $(1/\lambda_1)$. A similar equation holds for the SSH with the relationship between
542 SSH and pycnocline depth given by (5).

543 In Figure 9, the evolution of pycnocline depth and SSH along 50°N are compared
544 with the evolution of SSH anomalies from the AVISO dataset over the period 1993-2004
545 (satellite data start in 1993). The evolution of SSH anomalies obtained using the Ekman
546 pumping model (4) and the Rossby wave model (8) over the same period are also shown
547 for comparison. Pycnocline depth values are converted to SSH units using (5), so that all
548 the fields can be plotted in the same units (cm) and with a similar contour interval.

549 The SSH anomalies from the altimeter (Figure 9c) show a clear indication of
550 westward propagation at a speed very similar to the 0.8 cm s^{-1} used for the Rossby wave
551 model (Figure 9e), as seen from the comparable slope of the phase lines. Similar
552 propagating characteristics are seen in the SSH field from ROMS, whose hovmöller
553 diagram compares remarkably well with that from the AVISO data, given the presence of
554 internal variability that may differ in the model and observations. Pycnocline depth
555 anomalies, on the other hand, have a more stationary evolution, which has a good
556 resemblance with that obtained from the Ekman pumping model (Figure 9d). A close
557 inspection of Figures 9a and 9b reveals that anomalies generated around 140°W have a
558 much weaker signature in the pycnocline depth field vs. the SSH field in the center of the
559 basin (145°W - 165°W), so that westward propagation is much less obvious in the
560 pycnocline depth field. These conclusions derived from visual inspection can be

quantified using correlation analysis. In Figure 10, the evolution of the SSHs from AVISO and ROMS at each longitude, as well as the evolution of pycnocline depth from ROMS are correlated with the time series generated using both the Ekman and Rossby models along 50°N over the period 1993-2004. In the longitude range 143°W-163°W correlations between the SSHs from both ROMS and AVISO and those derived from the Ekman pumping model drop to values very close to zero (and even below zero for AVISO), and are much lower than the correlations with the SSHs obtained from the Rossby model, which tend to remain above 0.5. On the other hand, pycnocline depth from ROMS tends to be described comparably well by both simple models, as the correlations are much more similar across the basin, except for the 155°W-160°W and 171°W-178°W longitude bands, and east of 134°W, where the correlations with the Ekman pumping model drop to values lower than 0.3.

Along 50°N the evolution of SSH from ROMS is similar to that derived from altimeter observations, and the evolution of both modeled and observed SSHs clearly show westward Rossby wave propagation. Is similar agreement found at different latitudes? As an example, we show in Figure 11 hovmöller diagrams of pycnocline depth, SSH from ROMS and SSH from AVISO along 53°N. Along this latitude westward propagation is much less pronounced in all three fields, and is not observed all across the basin as at 50°N. In the AVISO data (Figure 11c) westward propagating features can be observed east of 140°W, and west of 155°W. This westward propagation close to the margins of the GOA may be associated with the propagation of eddies along the coast. In the model's fields (Figures 11a,b) westward propagation is less evident. As noted for the

evolution along 50°N , the correspondence between pycnocline depth anomalies and SSH anomalies in ROMS varies as a function of longitude, and large SSH signals, like the one centered around 155°W from 1993 to 2000 seem to have a much weaker pycnocline depth signature.

To further examine the relationship between pycnocline depth and SSH we show, in Figure 12, the spatial distribution of the correlation between the two fields. Correlations are larger than 0.7 over a broad area, but drop to values below 0.7 in the centre of the gyre. The average correlation between the two fields in the region 155°W - 145°W , 52°N - 54°N (dot-dash box in Figure 12) is ~ 0.6 . Why is the SSH-pycnocline depth correspondence lower in the centre of the gyre? Since the pycnocline is shallower in this region, one may think that the evolution of pycnocline depth is affected by mixed layer processes and not only consists of dynamical signals excited by the varying wind forcing. In Figure 13 we compare the evolution of pycnocline depth and SSH averaged in the box 155°W - 145°W , 52°N - 54°N . The largest discrepancies between the two time series are observed from 1960 to 1974, when SSH variations are much weaker, and sometimes of opposite sign, than pycnocline depth changes, and after 1990, when SSH anomalies are larger than pycnocline depth anomalies.

To elucidate the relationship between the evolution of SSH and pycnocline depth with the surface forcing, the time series of the Ekman pumping averaged over the same box is also shown in Figure 13. The correlation between pycnocline depth and Ekman pumping is 0.7, with the Ekman pumping leading by 4 months, while the correlation between SSH and W_E is only 0.36 when the Ekman pumping leads by 5 months. Notice, in particular, that the evolution of pycnocline depth from 1960 to 1974 tracks very closely the

evolution of W_E during the same period, while the evolution of SSH does not. Thus, pycnocline depth changes appear to be more directly controlled by the Ekman pumping forcing than SSH in the center of the Alaska Gyre. The SSH evolution may also be influenced by diabatic processes, while pycnocline depth, being further away from the surface, may primarily capture the dynamical signals associated with varying wind forcing. We plan to use sensitivity experiments where either anomalous wind forcing or anomalous buoyancy forcing is prescribed to clarify this point in a future study.

Are the SSH and pycnocline depth variations in the center of the Alaska gyre related to the PDO and NPGO? Figures 14a,b show the comparison between the time series of pycnocline depth and SSH, averaged over the box in Figure 12, with the NPGO index. Notice that the NPGO index is shown with sign reversed for ease of comparison. Positive NPGO corresponds to an intensification of the eastern limbs of both subtropical and subpolar gyres, and is associated with negative SSH and pycnocline depth anomalies in the GOA.

The correlation coefficient between pycnocline depth and NPGO is 0.69 when the NPGO index leads by one month. This correlation is statistically significant at the 95% level. The correlation coefficient between SSH variations and NPGO index is 0.54 when the NPGO leads SSH by two months, which is marginally significant at the 95% level. The comparison of both pycnocline depth and SSH time series with the PDO index (Figures 14c, d, respectively) shows a lower degree of agreement. Pycnocline depth variations are practically uncorrelated with the PDO index (correlation coefficient is 0.09), while SSH has a correlation coefficient of 0.39 (PDO leading by 7 months), which is only marginally significant at the 90% level. The box we have chosen lays in the area

of positive SSH anomalies of the PDO pattern, but is very close to the nodal line of that pattern. The lower agreement may be partly due to the position of the box relative to the spatial structure of the PDO mode. *Di Lorenzo et al.* [2008] have emphasized the large correlation between NPGO and coastal upwelling. Here we find that open ocean upwelling, as described by changes in pycnocline depth, is also related to the NPGO (but not the PDO).

Thus, the evolution of both pycnocline depth and SSH can be related to one of the leading North Pacific modes of climate variability. However, pycnocline depth is more directly correlated to local wind forcing, and appears to be the quantity that more clearly captures dynamical changes related to the NPGO mode of variability. This was not the case for the EKE along the western margin of the GOA, which was correlated with the PDO, but not the NPGO.

5. Summary and conclusions

In this paper we have used an eddy-permitting ocean model of the northeast Pacific to examine the role of eddies in the adjustment of the Gulf of Alaska circulation to changes in the surface wind forcing. We have also compared the dynamical information contained in the evolution of the sea surface height (SSH) field with that of pycnocline depth. Results from the eddy-permitting model are in agreement with the findings of a previous study which was based on a relatively coarse resolution global ocean model (CADM05) in that local Ekman pumping can explain a large fraction of both pycnocline and SSH

variability in the center of the Gulf of Alaska (GOA), and in part of the eastern and northern coastal regions.

Pycnocline depth and SSH changes associated with the 1976-77 climate shift are qualitatively similar to the pattern of pycnocline depth changes computed by CADM05: the pycnocline shoals in the center of the gyre and deepens along the coast, while the SSH field is higher along the coast, and lower in the interior after the shift. Due to the increased zonal gradients of pycnocline depth, the circulation is stronger after the climate shift. The standard deviation of SSH, as well as eddy kinetic energy (EKE), two measures of the intensity of the mesoscale eddy field, are also generally larger after the climate shift along the coastal areas.

SSH is usually considered the mirror image of pycnocline depth (scaled by the ratio of reduced gravity and gravity), and containing the same dynamical information. The comparison of SSH and pycnocline depth evolution reveals, however, subtle differences. At some latitudes, westward propagation is much clearer in the SSH field than in the pycnocline depth field, and the relationship with the surface forcing is not always the same. In the center of the Alaska gyre, the evolution of pycnocline depth is largely correlated with the local Ekman pumping, while the correlation between SSH and Ekman pumping is lower.

The local forcing is, in turn, part of large-scale patterns of atmospheric variability. The leading modes of SSH variability over the northeast Pacific, as defined by *Di Lorenzo et al.* [2008] include the Pacific Decadal Oscillation (PDO) and the North Pacific Gyre Oscillation (NPGO). Pycnocline depth variations in the central Gulf of Alaska are significantly correlated with the NPGO, while the relationship between SSH and NPGO

is more tenuous. The wind stress pattern associated with the positive phase of the NPGO (Figure 3b of *Di Lorenzo et al.* [2008]) shows positive zonal wind stress anomalies centered at approximately 45°N, which can be expected to be associated with positive (upwelling favorable) W_E anomalies around 50°N - 55°N. Pycnocline depth variations in that area are significantly correlated with W_E variations, which may be primarily associated with the NPGO mode of variability. *Di Lorenzo et al.* [2008] have stressed the connection between NPGO and coastal upwelling along the California current. Our results seem to indicate that this relationship also holds in the center of the GOA, where pycnocline depth changes are indicative of variations in open ocean upwelling.

The mesoscale eddy field in the Gulf of Alaska plays a fundamental role in the transport of iron and nutrients between the coastal regions and the open ocean, and eddy statistics is considered very important for biological processes. A major issue concerns the possible changes in eddy statistics that may occur due to global warming. The current generation of climate models used for climate change projections is run at a horizontal resolution that is unable to capture mesoscale eddies, so that information about eddy statistics changes will not be readily available.

Previous studies have shown that the eddy field in the eastern basin is related to the local wind forcing, so that downwelling favorable winds lead to a stronger Alaska current and a more energetic eddy field. Eddies in the western basin are generated by internal instabilities of the flow, or drifted from the eastern and northern formation sites, so that they are not expected to be related to the local wind forcing. In this study we have examined the relationship between the eddy kinetic energy (EKE) in the western basin and the leading modes of SSH variability. A statistically significant correlation is found

between EKE and the PDO, the mode of variability that seems to capture variations in the circulation strength. Thus, if climate models can realistically simulate the leading modes of climate variability in the northeast Pacific and their evolution in future climate scenarios, possible changes in some aspects of eddy statistics may be inferred from the large-scale climate changes.

Acknowledgments

This study was supported by the National Science Foundation (OCE-0452743, OCE-0452692, OCE-0452654, and NSF GLOBEC OCE-0606575). We thank the two anonymous Reviewers for their excellent and constructive comments and suggestions.

References

- Alexander, M. A., A. Capotondi, A. J. Miller, F. Chai, R. Brodeur, and C. Deser (2008), Decadal variability in the northeast Pacific in a physical-ecosystem model: Role of mixed-layer depth and trophic interactions, *J. Geophys. Res.*, 113, C02017, doi:10.1029/2007JC004359.
- Bond, N. A., J. E. Overland, M. Spillane, and P. Stabeno (2003), Recent shifts in the state of the North Pacific, *Geophys. Res. Lett.*, 30(23), 2183, doi:10.1029/2003GL018597.
- Capotondi, A., M. A. Alexander, C. Deser, and A. J. Miller (2005), Low-frequency pycnocline variability in the northeast Pacific, *J. Phys. Oceanogr.*, 35, 1403-1420.

718 Chelton, D. B., and R. E. Davis (1982), Monthly mean sea-level variability along the
 719 west coast of North America, *J. Phys. Oceanogr.*, 12, 757-784.

720 Chelton, D. B., R. A. deSzoeki, and M. G. Schlax (1998), Geographical variability of the
 721 first baroclinic Rossby radius of deformation, *J. Phys. Oceanogr.*, 28, 433-460.

722 Chhak, K. C., E. Di Lorenzo, P. Cummins, and N. Schneider (2008), Forcing of low-
 723 frequency ocean variability in the northeast Pacific, *J. Clim.*, submitted.

724 Combes, V., and E. Di Lorenzo (2007), Intrinsic and forced interannual variability of the
 725 Gulf of Alaska mesoscale circulation, *Prog. Oceanogr.*,
 726 doi:10.1016/j.pocean.2007.08.011.

727 Crawford, W. R., (2002), Physical characteristics of Haida eddies. *J. Oceanogr.*, 58, 703-
 728 713.

729 Crawford, W. R., J. Y. Cherniawsky, and M. G. G. Foreman (2000), Multi-year meanders
 730 and eddies in the Alaskan Stream as observed by TOPEX/Poseidon altimeter, *Geophys.*
 731 *Res. Lett.*, 27, 1025-1028.

732 Crawford, W. R., P. J. Brickley, T. D. Peterson, and A. C. Thomas (2005), Impact of
 733 Haida eddies on chlorophyll distribution in the eastern Gulf of Alaska, *Deep Sea Res.*
 734 *II*, 52, 975-989.

735 Crawford, W. R., P. J. Brickley, and A. C. Thomas (2007), Mesoscale eddies determine
 736 phytoplankton distribution in northern Gulf of Alaska, *Progress Oceanogr.*, 75, 287-
 737 303.

738 Cummins, P. F., and G. S. E. Lagerloef (2002), Low-frequency pycnocline depth
 739 variability at Ocean Weather Station P in the northeast Pacific, *J. Phys. Oceanogr.*, 32,
 740 3207-3215.

741 Cummins, P. F., and G. S. E. Lagerloef (2004), Wind-driven interannual variability over
 742 the northeast Pacific Ocean. *Deep-Sea Res.*, I, 51, 2105-2121.

743 Curchitser, E. N., D. B. Haidvogel, A. J. Hermann, E. L. Dobbins, T. M. Powell, and A.
 744 Kaplan (2005), Multi-scale modeling of the North Pacific Ocean: Assessment and
 745 analysis of simulated basin-scale variability (1996-2003), *J. Geophys. Res.*, 110.

746 Di Lorenzo, E., N. Schneider, K. M. Kobb, P. J. S. Frank, K. Chhak, A. J. Miller, J. C.
 747 McWilliams, S. J. Bograd, H. Arango, E. Curchitser, T. M. Powell, and P. Rivière
 748 (2008), North Pacific Gyre Oscillation links ocean climate and ecosystem change,
 749 *Geophys. Res. Lett.*, 35, L08607, doi:10.1029/2007GL032838.

750 Doney, S. C., S. Yeager, G. Danabasoglu, W. G. Large, and J. C. McWilliams (2003),
 751 Modeling global oceanic interannual variability (1958-1997): Simulation design and
 752 model-data evaluation, NCAR Tech. Note NCAR/TN-452+STR.

753 Ducet, N., P. Y. Le Traon, and G. Reverdin (2000), Global high-resolution mapping of
 754 ocean circulation from TOPEX/Poseidon and ERS-1 and -2, *J. Geophys. Res.*, 105,
 755 19,477-19,498.

756 Emery, W. J., and K. Hamilton (1985), Atmospheric forcing of interannual variability in
 757 the northeast Pacific Ocean, *J. Geophys. Res.*, 90, 857-868.

758 Enfield, D. B., and J. S. Allen (1980), On the structure and dynamics of monthly mean
 759 sea level anomalies along the Pacific coast of North and South America, *J. Phys.*
 760 *Oceanogr.*, 10, 557-578.

761 Freeland, H. J., K. Denman, C. S. Wong, F. Whitney, and R. Jacques (1997), Evidence of
 762 change in the winter mixed layer in the northeast Pacific Ocean, *Deep-Sea Res.*, 44,
 763 2117-2129.

764 Haidvogel, D. B., G. Arango, et al. (2000), Model evaluation experiments in the North
 765 Atlantic Basin: Simulations in nonlinear terrain-following coordinates, *Dyn. Atmos.*
 766 *Ocean*, 32, 239-281.
 767 Kalney, E., and Coauthors (1996), The NCEP/NCAR 40-year Reanalysis Project, *Bull.*
 768 *Amer. Meteor. Soc.*, 77, 437-471.
 769 Killworth, P. D., D. B. Chelton, and R. A. de Szoeke (1997), The speed of observed and
 770 theoretical long extratropical planetary waves, *J. Phys. Oceanogr.*, 27, 1946-1966.
 771 Ladd, C., P. Stabeno, and E. D. Cokelet (2005), A note on cross-shelf exchange in the
 772 northern Gulf of Alaska, *Deep-Sea Res. II*, 52, 667-679.
 773 Ladd, C. (2007), Interannual variability of the Gulf of Alaska eddy field. *Geophys. Res.*
 774 *Lett.*, 34, doi:10.1029/2007GL029478.
 775 Ladd, C., C. W. Mordy, N. B. Kachel, and P. J. Stabeno (2007), Northern Gulf of Alaska
 776 eddies and associated anomalies, *Deep-Sea Res. I*, 54, 487-509.
 777 Lagerloef, G. S. E. (1995), Interdecadal variations in the Alaska gyre, *J. Phys.*
 778 *Oceanogr.*, 25, 2242-2258.
 779 Large, W. G., and S. Pond (1982), Sensible and latent heat flux measurements over the
 780 ocean, *J. Phys. Oceanogr.*, 12, 464-482.
 781 Large, W. G., G. Danabasoglu, and S. C. Doney (1997), Sensitivity to surface forcing
 782 and boundary-layer mixing in a global ocean model: Annual mean climatology, *J.*
 783 *Phys. Oceanogr.*, 27, 2418-2447.
 784 Large, W. G., J. C. McWilliams, P. R. Gent, and F. O. Bryan (2001), Equatorial
 785 circulation of a global ocean climate model with anisotropic horizontal viscosity, *J.*
 786 *Phys. Oceanogr.*, 31, 518-536.

787 Le Traon, P. Y., and G. Dibarboure (1999), Mesoscale mapping capabilities of multi-
788 satellite altimeter missions, *J. Atmos. Oceanic Technol.*, 16, 1208-1223.

789 Levitus, S., R. Burgett, and T. Boyer (1994), World Ocean Atlas 1994. NOAA Atlas
790 NESDIS 4, US Government Printing Office, Washington, D. C., pp 3-4.

791 Mantua, N. J., S. Hare, Y. Zhang, J. M. Wallace, and R. Francis, (1997), A Pacific
792 interdecadal climate oscillation with impacts on salmon production. *Bull. Amer.*
793 *Meteor. Soc.*, 78, 1069-1079.

794 Marchesiello, P., J. C. McWilliams, and A. Shchepetkin (2003), Equilibrium structure and
795 dynamics of the California Current System, *J. Phys. Oceanogr.*, 33, 753-783.

796 Miller, A. J., E. Di Lorenzo, D. J. Neilson, H.-J. Kim, A. Capotondi, M. A. Alexander, S.
797 J. Bograd, F. B. Schwing, R. Mendelssohn, K. Hedstrom and D. L. Musgrave (2005),
798 Interdecadal changes in mesoscale eddy variance in the Gulf of Alaska circulation:
799 possible implications for the Steller sea lion decline, *Atmosphere-Ocean*, 43, 231-240.

800 Meyers, S. D., and S. Basu (1999), Eddies in the eastern Gulf of Alaska from
801 TOPEX/POSEIDON altimetry, *J. Geophys. Res.*, 104, 13333-13343.

802 Nitta, T., and S. Yamada (1989), Recent warming of tropical SST and its relationship to
803 the Northern Hemisphere circulation, *J. Meteor. Soc. Japan*, 67, 375-383.

804 Okkonen, S. R., G. A. Jacobs, E. J. Metzger, H. E. Hurlburt, and J. F. Shriver (2001),
805 Mesoscale variability in the boundary current of the Alaska Gyre, *Continental Shelf*
806 *Res.*, 21, 1219-1236.

807 Okkonen, S. R., T. J. Weingartner, S. L. Danielson, D. L. Musgrave, and G. M. Schmidt
808 (2003), Satellite and hydrographic observations of eddy-induced shelf-slope exchange
809 in the northwestern Gulf of Alaska, *J. Geophys. Res.- Oceans*, 108.

810 Qiu, B. (2002), Large-scale variability in the midlatitude subtropical and subpolar North
811 Pacific Ocean: Observations and causes, *J. Phys. Oceanogr.*, 32, 353-375.

812 Shchepetkin, A. F., and J. C. McWilliams (2005), The regional oceanic modeling system
813 (ROMS): A split-explicit, free-surface, topography-following coordinate oceanic
814 model, *Ocean Modelling*, 9, 347-404.

815 Smith, T. M., and R. W. Reynolds (2004), Improved extended reconstruction of SST
816 (1854 -1997), *J. Clim.*, 17, 2466-2477.

817 Spencer, R. W. (1993), Global oceanic precipitation from the MSU during 1979-91 and
818 comparison to other climatologies, *J. Climate*, 6, 1301-1326,

819 Tabata, S. (1982), The anticyclonic, baroclinic eddy off Sitka, Alaska, in the northeast
820 Pacific Ocean, *J. Phys. Oceanogr.*, 12, 1260-1282.

821 Trenberth, K. E., and J. W. Hurrell (1994), Decadal atmosphere-ocean variations in the
822 Pacific. *Climate Dyn.*, 9, 303-319.

823 Xie, P., and P. A. Arkin (1996), Analyses of global monthly precipitation using gauge
824 observations, satellite estimates, and numerical model predictions, *J. Climate*, 9, 840-
825 858.

826 Yasuda, T., and K. Hanawa (1997): Decadal changes in mode waters in the midlatitude
827 North Pacific, *J. Phys. Oceanogr.*, 27, 858-870.

828

829

Figure captions

Figure 1. a) Time mean pattern of SSH from ROMS over the total duration of the ROMS simulation. Contour interval is 5 cm. b) Time mean pycnocline depth from ROMS. The 27.0 isopycnal is used as proxy for pycnocline depth. Contour interval is 20 m. Blue shading is for negative values, while orange shading indicates positive values.

Figure 2. Ekman pumping difference between Period 2 (1977-1997) and Period 1 (1958-1975). Units are cm/s. The locations of Queen Charlotte Island (Q), Sitka (S), Yakutat (Y), and Kodiak Island (K) are also indicated.

Figure 3. a) Difference in pycnocline depth (m) between the period 1977-1997 (P2) and the period 1958-1975 (P1) from the NCOM simulation. b) Same as in a), but for the ROMS simulation. c) Difference in SSH (cm) between P2 and P1 from ROMS. Orange shading is used for positive values (deeper pycnocline, higher SSH), while blue shading is for negative values (shallower pycnocline, negative SSH). “P” and “G” in a) indicate the location of station Papa (50°N, 145°W), and station GAK1 (59°N, 149°W).

Figure 4. a) Comparison of pycnocline depth from ROMS (black line) and NCOM (green line) with the observed pycnocline depth at Papa (blue line). b) Comparison of pycnocline depth from ROMS (black line) and NCOM (green line) with the observed pycnocline depth at GAK1 (blue line). c) Comparison of SSH (converted to pycnocline

depth units using equation 5, black line) with the observed pycnocline depth at Papa (blue line). d) Comparison of SSH with the observed pycnocline depth at GAK1. SSH from NCOM is not available. All values are in meters.

Figure 5. a) Changes in standard deviation of SSH (cm) and pycnocline depth (m) associated with the 1976-77 climate shift. The changes were computed as the differences between P2 (1977-1997), and P1 (1958-1975).

Figure 6. a) Mean surface total kinetic energy (TKE) in ROMS over the total duration of the integration (1950-2004) Contour interval is $100 \text{ cm}^2\text{s}^{-2}$. Values larger than $100 \text{ cm}^2\text{s}^{-2}$ are shaded. b) Mean surface eddy kinetic energy (EKE) in ROMS (1950-2004). Contour interval is $20 \text{ cm}^2\text{s}^{-2}$, and values larger than $20 \text{ cm}^2\text{s}^{-2}$ are shaded. c) EKE from AVISO (1993-2004), based on monthly averages of SSH anomalies. Contour interval is $20 \text{ cm}^2\text{s}^{-2}$, and values larger than $20 \text{ cm}^2\text{s}^{-2}$ are shaded. d) EKE difference between P2 (1977-1997) and Period 1 (1958-1975). Contour interval is $10 \text{ cm}^2\text{s}^{-2}$. Orange shading indicates positive values, while blue shading is for negative values.

Figure 7. Comparison of the EKE in the western GOA (dot-dash line) with a) the PDO, and b) the NPGO indices (solid lines). The EKE index is computed by averaging the EKE over the area where the mean EKE is larger than $1.0 \text{ cm}^2\text{s}^{-2}$, between 148°W and 165°W , and north of 52°N . This mainly capture EKE variations along the Alaskan Stream. The correlation coefficient between EKE and PDO index is 0.55, when the PDO leads the EKE by 1 month, while the correlation coefficient with the NPGO is only 0.22.

875

876 **Figure 8.** a) Maximum correlation, as a function of λ , between the pycnocline depth
877 computed using the local Ekman pumping model, and the pycnocline depth from ROMS.
878 Contour interval is 0.1. Values larger than 0.5 are shaded. b) Values of λ^{-1} (in months)
879 yielding the correlations in a). Values are shown only over the areas where correlations in
880 a) are larger than 0.5. Contour interval is 4 months for values lower than 20 months, and
881 20 months for values larger than 20 months. c) Same as a), but for SSH. d) Same as in b),
882 but for SSH.

883

884 **Figure 9.** a) Hovmöller diagram of pycnocline depth from ROMS along 50°N.
885 Pycnocline depth has been converted to SSH units using equation (5). b) Hovmöller
886 diagram of SSH from ROMS along 50°N, c) Same as b), but for SSH from the AVISO
887 archive, d) Evolution of SSH along 50°N obtained using the Ekman pumping model, and
888 e) SSH along 50°N from the Rossby wave model. Contour interval is all panels is 2 cm/s.

889

890 **Figure 10.** a) Correlation between AVISO SSH with the SSH from the Ekman pumping
891 model (solid), and the Rossby wave model (dot-dash) along 50°N and over the period
892 1993-2004. b) Same as a), but for ROMS SSH. c) Same as a), but for ROMS pycnocline
893 depth.

894

895 **Figure 11.** Hovmöller diagram of pycnocline depth (a), SSH from ROMS (b), and SSH
896 from AVISO (c) along 53°N. Pycnocline depth has been converted to SSH units using

equation (5). Contour interval is 2 cm. Blue shading is for negative values (shallower pycnocline, negative SSHs), while orange shading is for positive values (deeper pycnocline, positive SSH anomalies).

Figure 12. Instantaneous correlations between pycnocline depth and SSH in ROMS. Contour interval is 0.1. Values larger than 0.7 are shaded. The dot-dash box shows the area where averaged time series of the two fields are computed and compared.

Figure 13. Comparison between the time series of pycnocline depth (black line), SSH (blue line), and Ekman pumping (red line) averaged over the box shown in Figure 12. All time series are normalized by their standard deviations. Notice that the Ekman pumping W_E is shown with sign reversed for ease of comparison. The correlation coefficient between pycnocline depth and Ekman pumping is 0.70, when the Ekman pumping leads by 4 months, while the correlation coefficient of SSH and W_E is 0.36 when W_E leads by 5 months.

Figure 14. a) Comparison of pycnocline depth (black line) from ROMS in the box shown in Figure 12 with the NPGO index (red line). The NPGO index is shown with sign reversed for ease of comparison. The correlation coefficient between the two time series is 0.69 when the NPGO index leads by one month. b) Same as in a), but for SSH (blue line). The correlation coefficient between the two time series is 0.54 when the NPGO leads by two months. c) Comparison of pycnocline depth from ROMS in the box shown in Figure 12 with the PDO index (green line). The correlation coefficient is only 0.09. d)

920 Same as c), but for SSH (green line). The correlation coefficient between SSH and PDO
921 is 0.39 when the PDO leads by 7 months. All time series have been normalized by their
922 standard deviations.

923

924

925

926

927

928

929

930

931

932

933

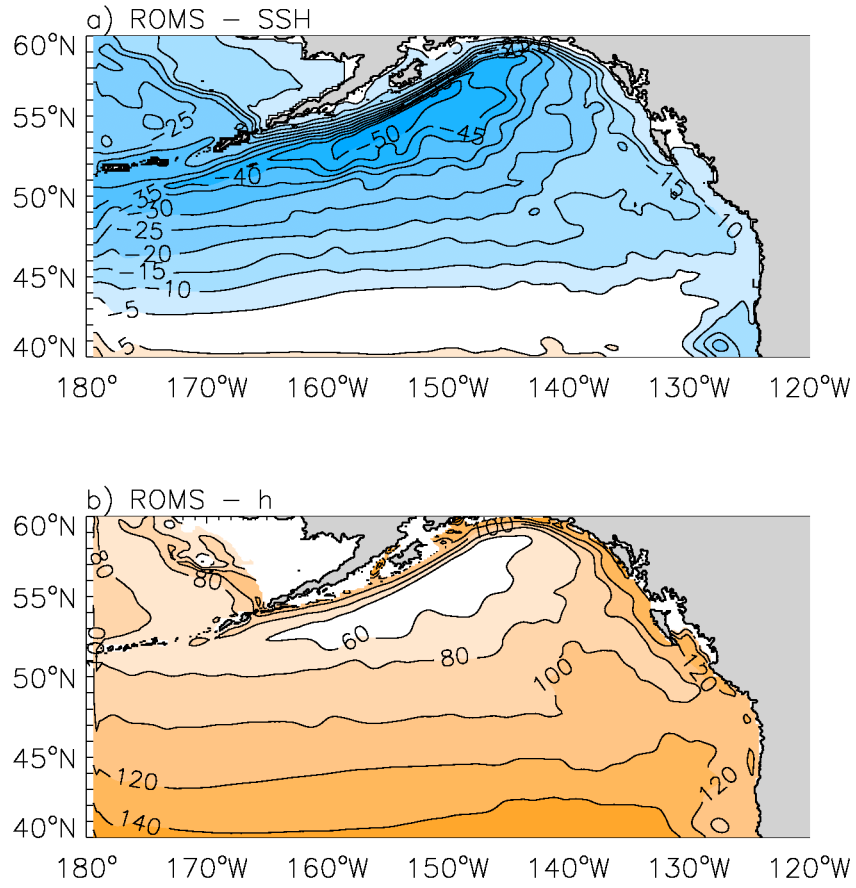
934

935

936

937

938



938

Figure 1. a) Time mean pattern of SSH from ROMS over the total duration of the ROMS simulation. Contour interval is 5 cm. b) Time mean pycnocline depth from ROMS. The 27.0 isopycnal is used as proxy for pycnocline depth. Contour interval is 20 m. Blue shading is for negative values, while orange shading indicates positive values.

939

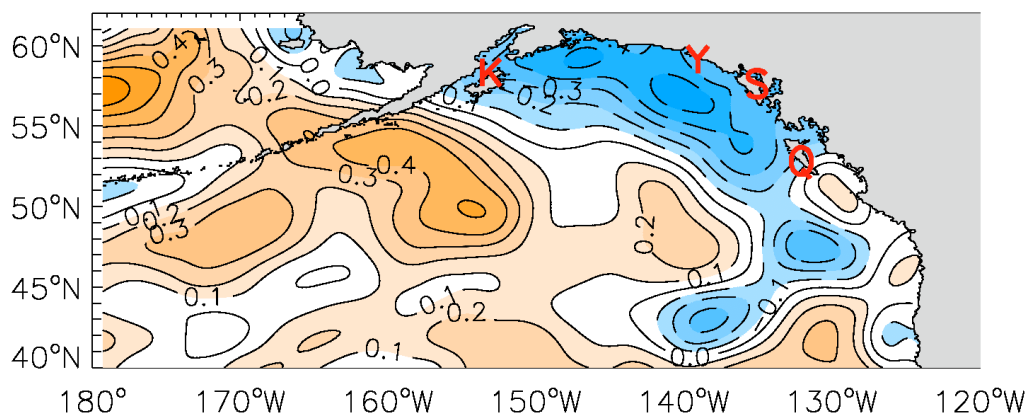


Figure 2. Ekman pumping difference between Period 2 (1977-1997) and Period 1 (1958-1975). Units are cm/s. The locations of Queen Charlotte Island (Q), Sitka (S), Yakutat (Y), and Kodiak Island (K) are also indicated.

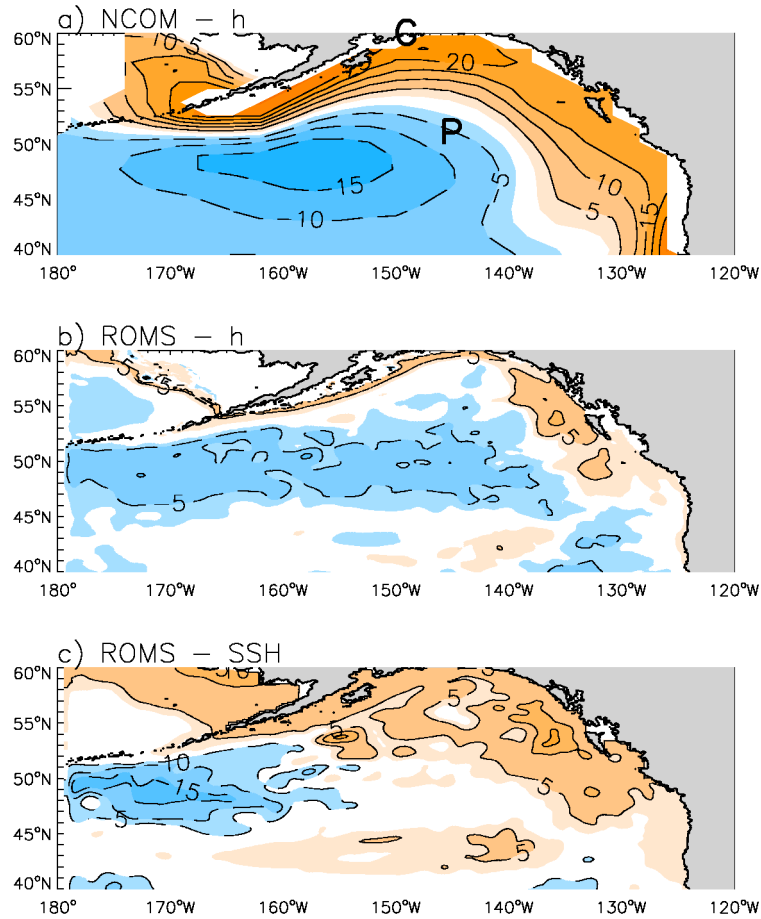


Figure 3. a) Difference in pycnocline depth (m) between the period 1977-1997 (P1) and the period 1958-1975 (P2) from the NCOM simulation. b) Same as in a), but for the ROMS simulation. c) Difference in SSH (cm) between P2 and P1 from ROMS. Orange shading is used for positive values (deeper pycnocline, higher SSH), while blue shading is for negative values (shallower pycnocline, negative SSH). “P” and “G” in a) indicate the location of station Papa (50°N, 145°W), and station GAK1 (59°N, 149°W).

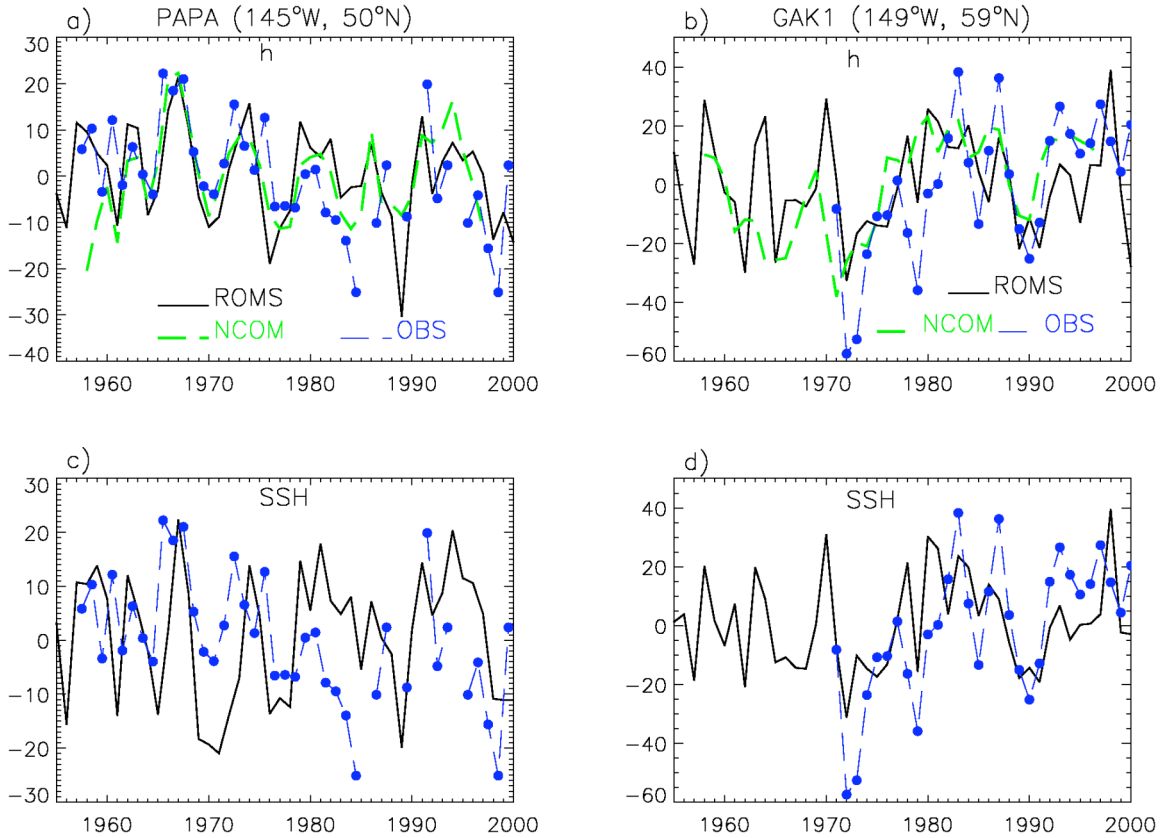


Figure 4. a) Comparison of pycnocline depth from ROMS (black line) and NCOM (green line) with the observed pycnocline depth at Papa (blue line). b) Comparison of pycnocline depth from ROMS (black line) and NCOM (green line) with the observed pycnocline depth at GAK1 (blue line). c) Comparison of SSH (converted to pycnocline depth units using equation 5, black line) with the observed pycnocline depth at Papa (blue line). d) Comparison of SSH with the observed pycnocline depth at GAK1. SSH from NCOM is not available. All values are in meters.

946

947
948

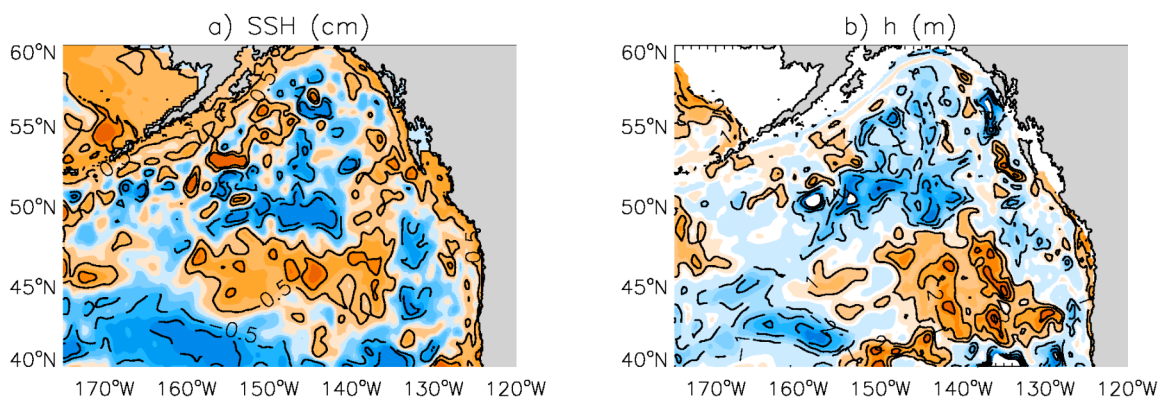


Figure 5. a) Changes in standard deviation of SSH (cm) and pycnocline depth (m) associated with the 1976-77 climate shift. The changes were computed as the differences between P2 (1977-1997), and P1 (1958-1975).

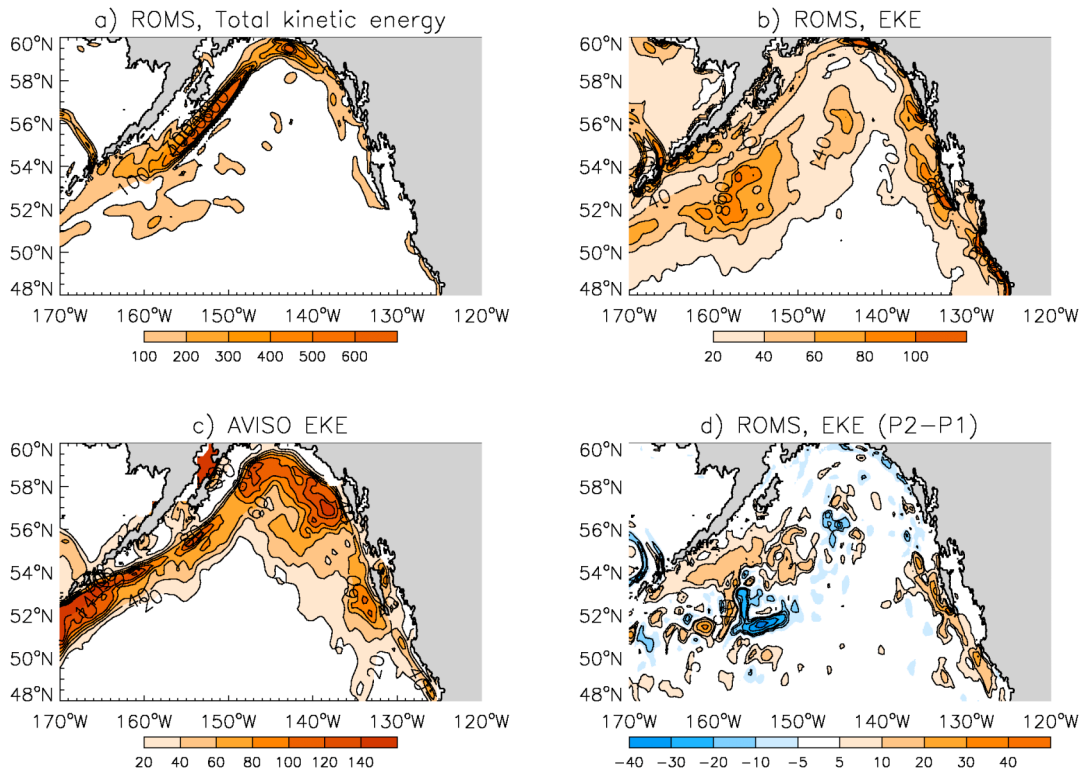
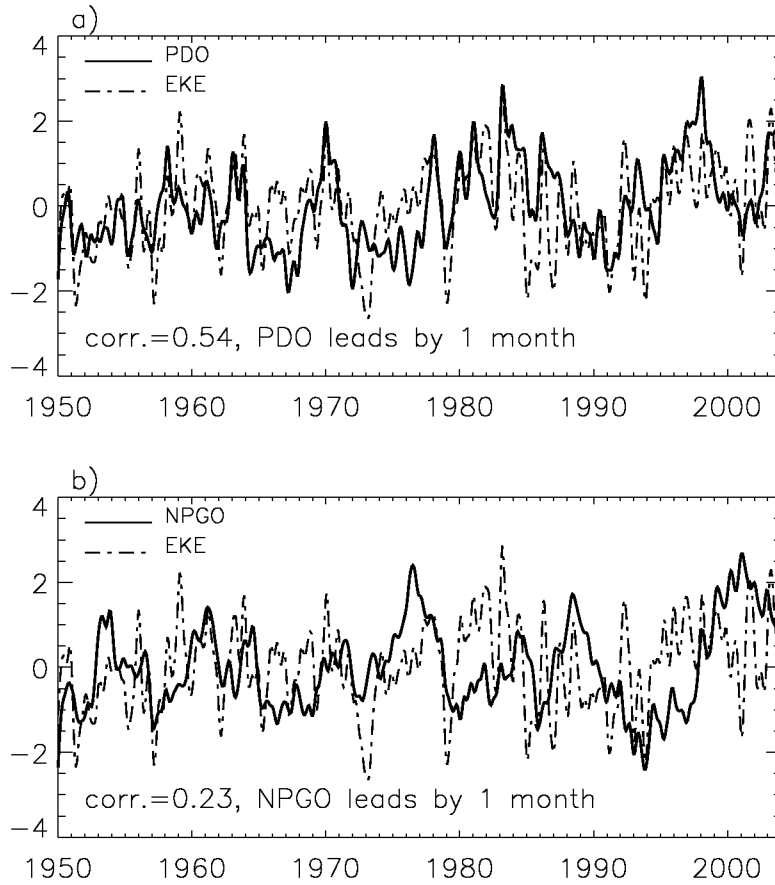


Figure 6. a) Mean surface total kinetic energy (TKE) in ROMS over the total duration of the integration (1950-2004). Contour interval is $100 \text{ cm}^2\text{s}^{-2}$. Values larger than $100 \text{ cm}^2\text{s}^{-2}$ are shaded. b) Mean surface eddy kinetic energy (EKE) in ROMS (1950-2004). Contour interval is $20 \text{ cm}^2\text{s}^{-2}$, and values larger than $20 \text{ cm}^2\text{s}^{-2}$ are shaded. c) EKE from AVISO (1993-2004), based on monthly averages of SSH anomalies. Contour interval is $20 \text{ cm}^2\text{s}^{-2}$, and values larger than $20 \text{ cm}^2\text{s}^{-2}$ are shaded. d) EKE difference between P2 (1977-1997) and Period 1 (1958-1975). Contour interval is $10 \text{ cm}^2\text{s}^{-2}$. Orange shading indicates positive values, while blue shading is for negative values.



950

Figure 7. Comparison of the EKE in the western GOA (dot-dash line) with a) the PDO, and b) the NPGO indices (solid lines). The EKE index is computed by averaging the EKE over the area where the mean TKE is larger than $100.0 \text{ cm}^2 \text{ s}^{-2}$, between 148°W and 165°W , and north of 52°N . This mainly capture EKE variations along the Alaskan Stream. The correlation coefficient between EKE and PDO index is 0.54, when the PDO leads the EKE by 1 month, while the correlation coefficient with the NPGO is only 0.23.

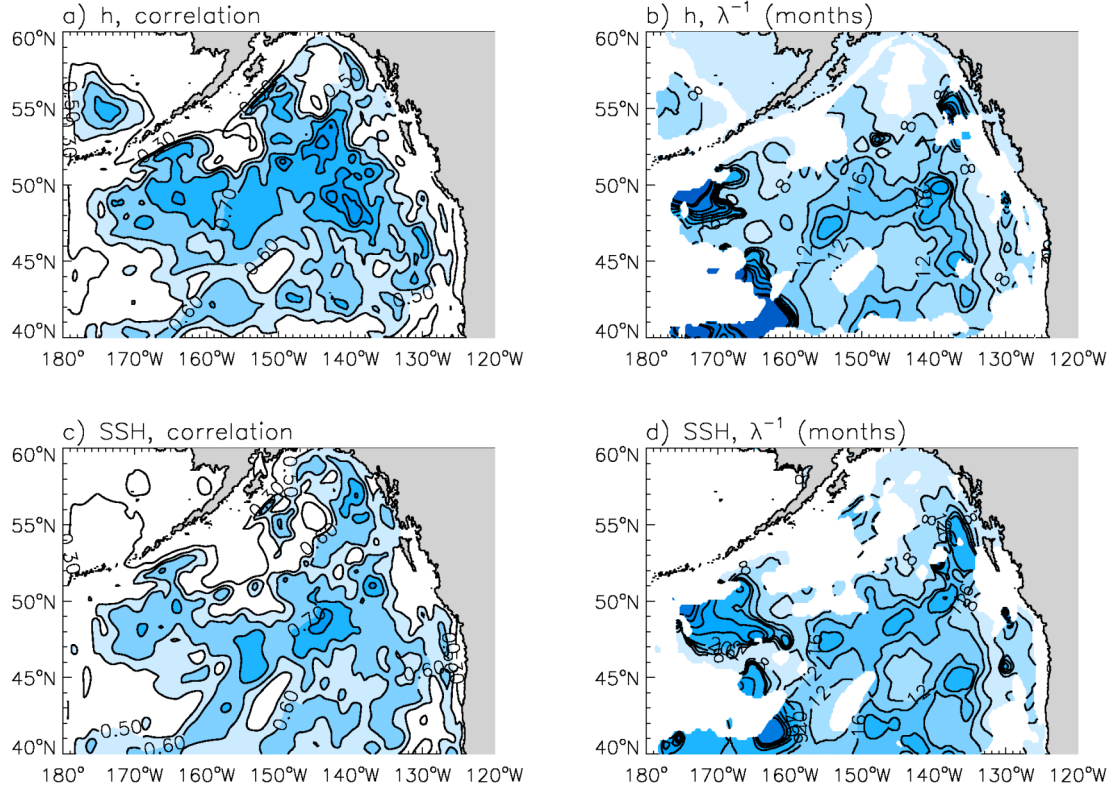


Figure 8. a) Maximum correlation, as a function of λ , between the pycnocline depth computed using the local Ekman pumping model, and the pycnocline depth from ROMS. Contour interval is 0.1. Values larger than 0.5 are shaded. b) Values of λ^{-1} (in months) yielding the correlations in a). Values are shown only over the areas where correlations in a) are larger than 0.5. Contour interval is 4 months for values lower than 20 months, and 20 months for values larger than 20 months. c) Same as a), but for SSH. d) Same as in b), but for SSH.

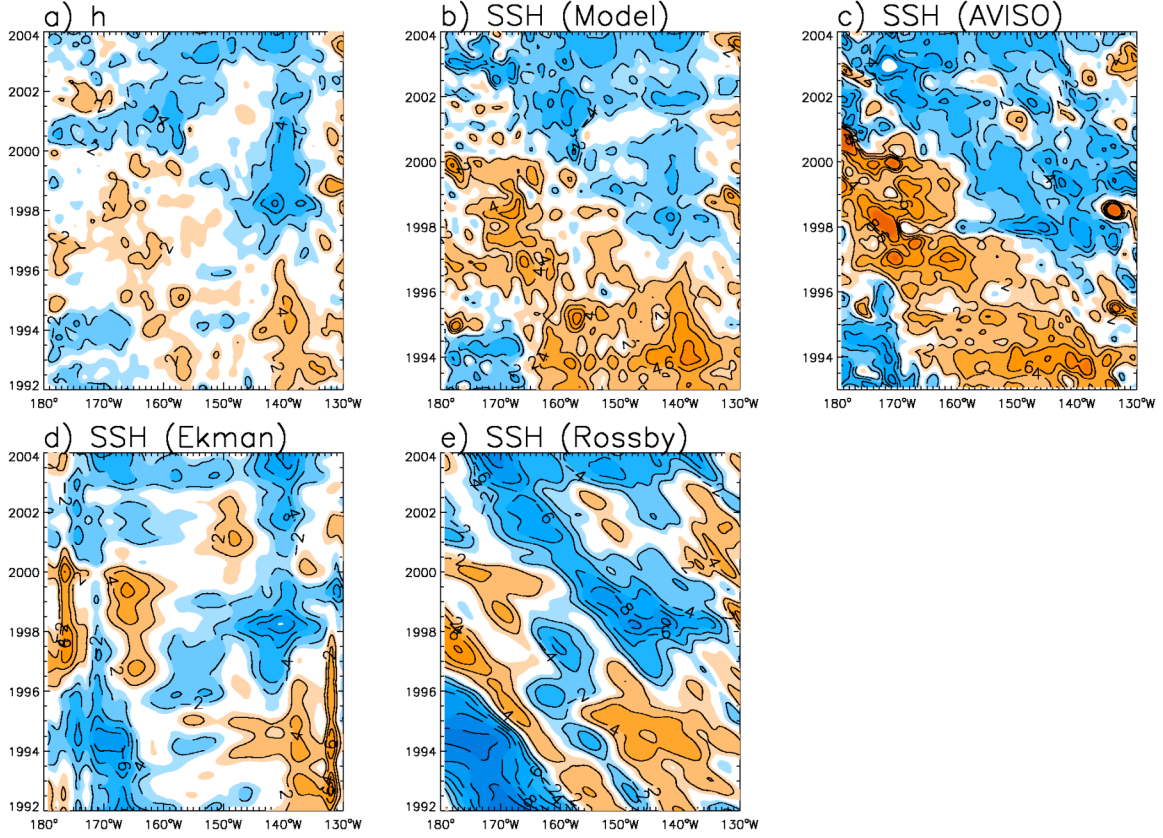


Figure 9. a) Hovmöller diagram of pycnocline depth from ROMS along 50°N. Pycnocline depth has been converted to SSH units using equation (5). b) Hovmöller diagram of SSH from ROMS along 50°N, c) Same as b), but for SSH from the AVISO archive, d) Evolution of SSH along 50°N obtained using the Ekman pumping model, and e) SSH along 50°N from the Rossby wave model. Contour interval in all panels is 2 cm/s.

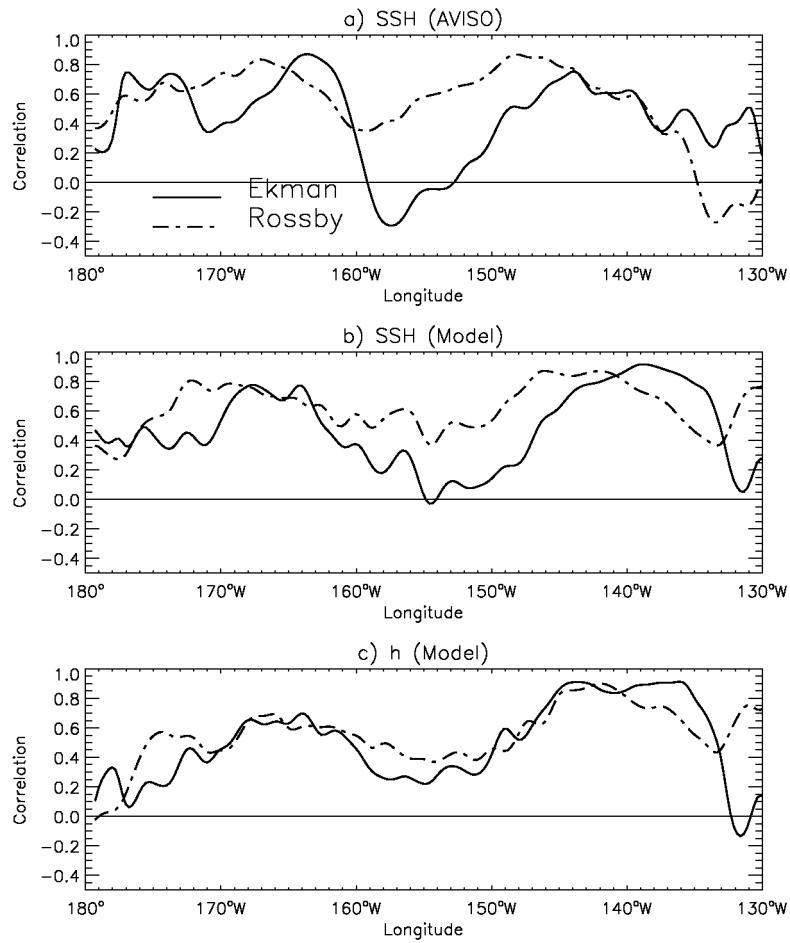


Figure 10. a) Correlation between AVISO SSH with the SSH from the Ekman pumping model (solid), and the Rossby wave model (dot-dash) along 50°N and over the period 1993-2004. b) Same as a), but for ROMS SSH. c) Same as a), but for ROMS pycnocline depth.

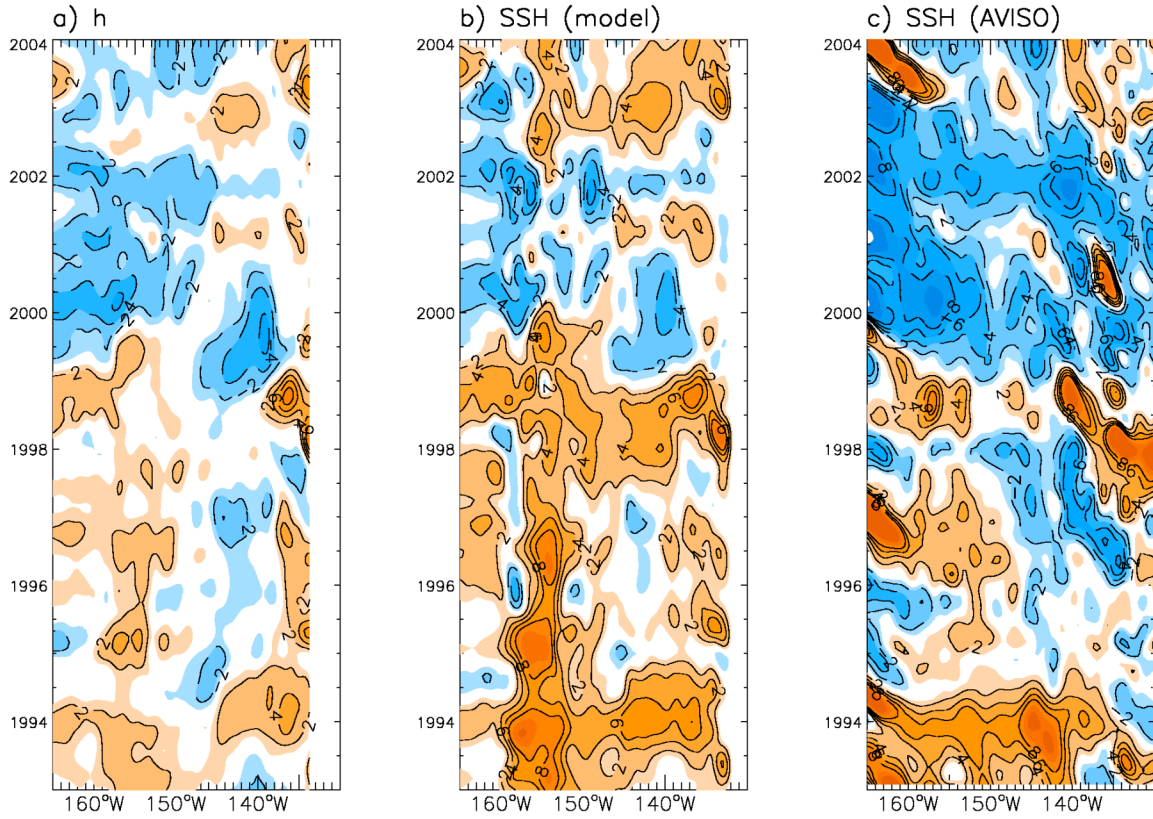


Figure 11. Hovmöller diagram of pycnocline depth (a), SSH from ROMS (b), and SSH from AVISO (c) along 53°N. Pycnocline depth has been converted to SSH units using equation (5). Contour interval is 2 cm. Blue shading is for negative values (shallower pycnocline, negative SSHs), while orange shading is for positive values (deeper pycnocline, positive SSH anomalies).

955

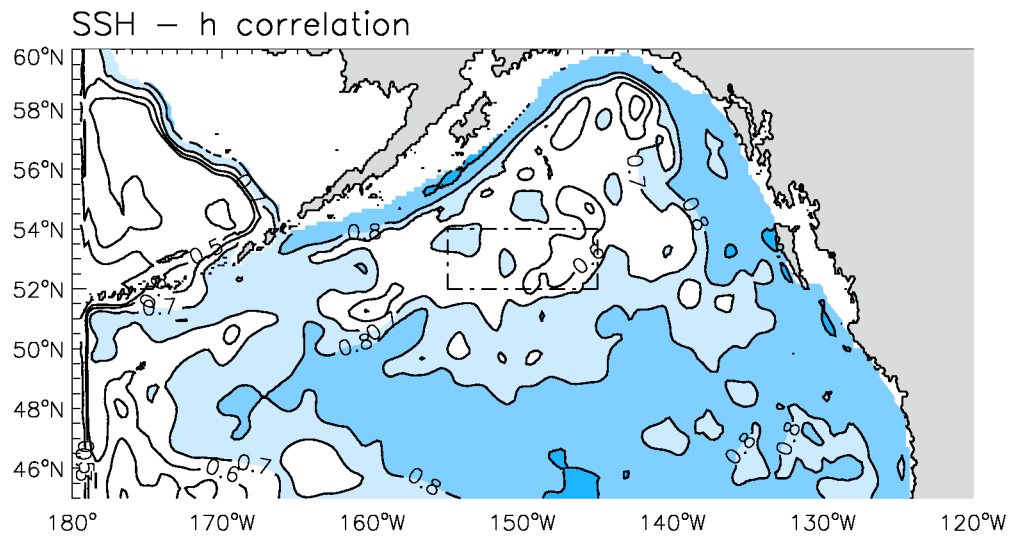
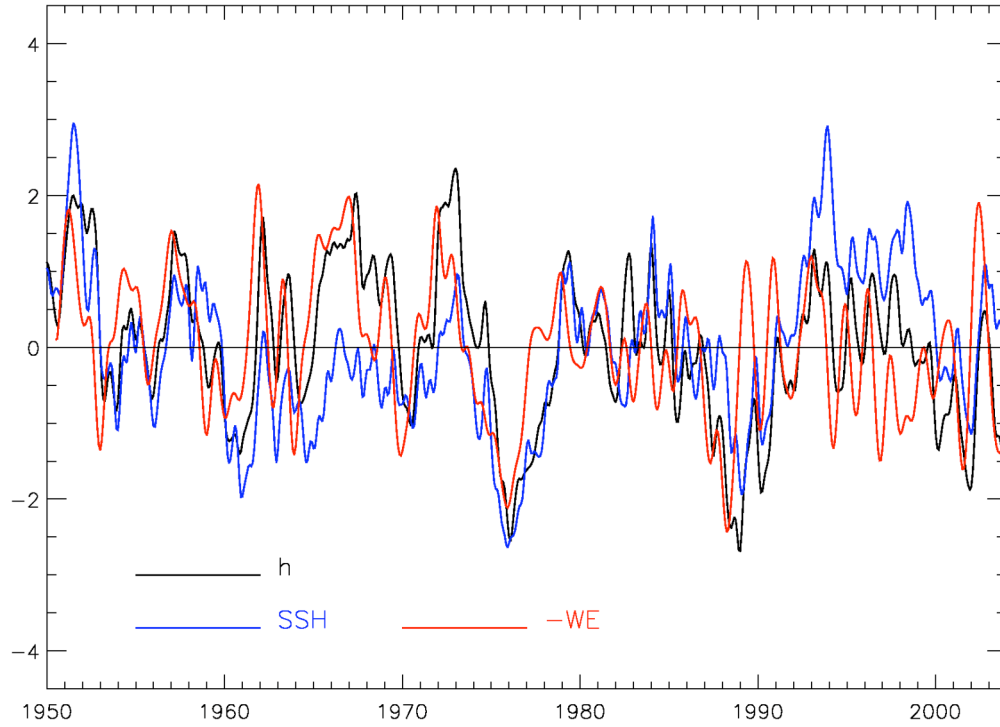


Figure 12. Instantaneous correlations between pycnocline depth and SSH in ROMS. Contour interval is 0.1. Values larger than 0.7 are shaded. The dot-dash box shows the area where averaged time series of the two fields are computed and compared.

956
957



958

Figure 13. Comparison between the time series of pycnocline depth (black line), SSH (blue line), and Ekman pumping (red line) averaged over the box shown in Figure 12. All time series are normalized by their standard deviations. Notice that the Ekman pumping W_E is shown with sign reversed for ease of comparison. The correlation coefficient between pycnocline depth and Ekman pumping is 0.70, when the Ekman pumping leads by 4 months, while the correlation coefficient of SSH and W_E is 0.36 when W_E leads by 5 months.

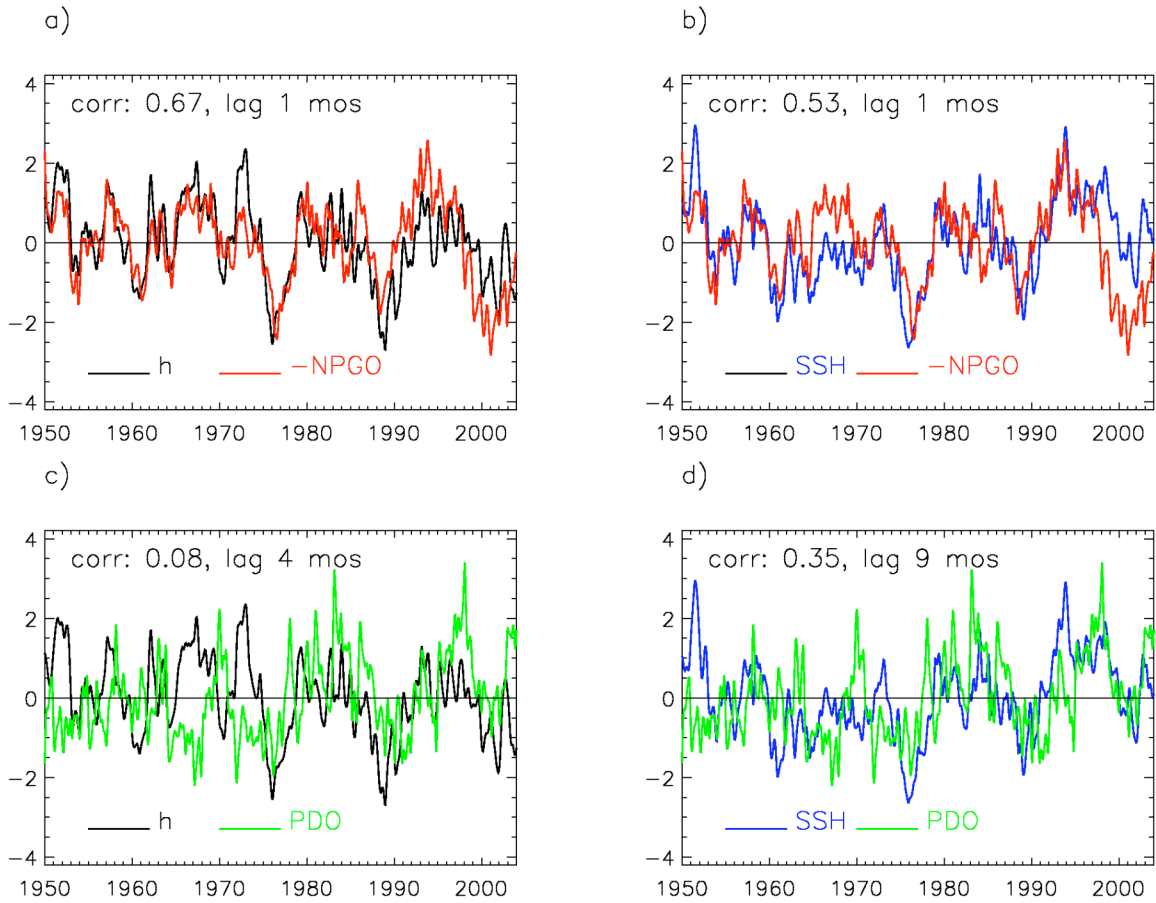


Figure 14. a) Comparison of pycnocline depth (black line) from ROMS in the box shown in Figure 12 with the NPGO index (red line). The NPGO index is shown with sign reversed for ease of comparison. The correlation coefficient between the two time series is 0.69 when the NPGO index leads by one month. b) Same as in a), but for SSH (blue line). The correlation coefficient between the two time series is 0.54 when the NPGO leads by two months. c) Comparison of pycnocline depth from ROMS in the box shown in Figure 12 with the PDO index (green line). The correlation coefficient is only 0.09. d) Same as c), but for SSH (green line). The correlation coefficient between SSH and PDO is 0.39 when the PDO leads by 7 months. All time series have been normalized by their standard deviations.